Signatures of Target Performance and Mixing in Titanium-Doped Target Implosions on OMEGA

In recently published work we discussed the signatures of mixing[1] and of target performance[2] provided by incorporating a titanium-doped layer within the shell of imploding targets. We report here on the results of an experiment on OMEGA using such targets. We observe the predicted absorption features formed by the titanium layer: absorption lines due to 1*s*–2*p* transitions in titanium ions of incomplete *L* shell, as well as *K*-edge absorption in cold titanium. We also observe oscillations due to extended x-ray absorption fine structure (EXAFS) above the Ti *K* edge. The observed spectra are simulated by a radiative-transport model that uses *LILAC* profiles and OPLIB opacity values. The observed core temperature and shell areal density are found to fall short of the one-dimensional predicted values. We attribute this shortfall to a lack of irradiation symmetry, which leads to hydrodynamic instability and mixing [distributed phase plates (DPP's) were not used in this experiment, although the SSD modulator was activated]. The introduction of a sharp density jump at the interfaces of the titanium layer introduces a Rayleigh-Taylor (RT) unstable layer, which makes the target more unstable. Signatures of mixing include the emission of the He-α line of Ti^{+20} due to titanium migrating to the core, as well as the EXAFS spectrum indicating cold titanium close to peak compression. The spectral signatures due to the titanium layer are shown to provide very useful signatures of target performance.

A titanium layer was placed within a polymer-shell target, between a mandrel and an overcoat layer. The overcoat is much thicker than the laser-ablated layer to prevent emission of titanium lines from laser heating. Likewise, the titanium layer was sufficiently far from the inner-shell interface to ensure that the titanium lines are not emitted in the absence of mixing.[1] The titanium layer is thus cold for the most part and should give rise to absorption lines.[3] The measured area enclosed within the absorption lines yields the areal density of the titanium and, by implication, of the total compressed shell. The intensity distribution of the absorption lines yields the temperature of the cold titanium layer. Additionally, the intensity slope of the continuum at higher photon energies yields the core temperature. These parameters are deduced from the measured spectra and compared with simulation predictions. Highly performing targets require only a low percentage (~1%) of titanium doping to give significant absorption;[2] the need to use a pure-titanium layer in this experiment is an indication of lower compression.

The sharp density jump at the interfaces of the titanium layer becomes unstable during acceleration and deceleration; however, a thin layer cannot support unstable modes of long wavelength. A reduction factor multiplying the RT growth rate, due to the finite thickness of an unstable layer, has been derived by Landau and Lifshitz.[4] One-dimensional code simulations of shot 8207 (see below) show that during the acceleration phase (when the shell and Ti layer are still thin) the reduction factor ranges from ~0.2 to ~0.5 for modes $\ell = 10$ to $\ell = 50$. Thus, the contribution of the titanium interface to the overall RT growth should be small.

In this article we concentrate on a single shot on the OMEGA laser[5]—shot No. 8207. The target was a polymer shell of 882-μm inner diameter and 4.6-μm thickness, coated with a 0.3-μm layer of titanium, a 15-μm layer of polymer, and finally a 0.1-μm layer of aluminum as a shinethrough barrier.[6] The fill gas was atmospheric air. The 19.9-kJ laser pulse had a 1-ns flat top (to within ±5%) with 150-ps rise and fall times. SSD[7] was used in this experiment, but not DPP's.[8]

Experimental Results

Spectrally dispersed images were obtained with a Kirkpatrick-Baez x-ray microscope of resolution ≤5 μm, fitted with a dispersing grating.[9] The images show a highly nonuniform core of ~60-μm FWHM, indicating an unstable implosion. This is further indicated by the spectral results discussed below.

The x-ray spectrum in the range of ~4 to 9 keV was recorded by a Ge(111) crystal spectrometer fitted with a 100-μm-wide spatially resolving slit. The slit acts to discriminate core radiation from coronal emission. The calibrated x-ray spectrum obtained with a Ge(111) diffracting crystal is shown in Fig. 70.38. Ti absorption lines are seen around 4.6 keV as well

as absorption above the Ti *K* edge at 4.966 keV. These absorption features take place when the radiation emitted by the hot, compressed core is absorbed by the colder Ti layer within the shell. The calibration procedure is explained in more detail in Ref. 10. For the calibration of the Kodak DEF film we relied on the measurements and modeling of Henke *et al.*;[11] for the calibration of the Ge(111) crystal we relied on the measurements of Burek and Yaakobi,[12] which agree well with the Darwin-Prins model calculations of Henke *et al.*[13] Figure 70.39 shows the measured and calculated crystal reflectivity. It should be noted that the crystal sensitivity is a weak function of energy in the range of interest (4 to 8 keV). In Fig. 70.40 we magnify the part of the spectrum showing various absorption features that are of particular interest in this experiment. As explained below, the lines around 4.6 keV are absorbed within a cool titanium layer (T_e ~200 to 500 eV), whereas radiation above the Ti *K* edge at 4.966 keV is absorbed by much colder titanium. The EXAFS oscillations also indicate cold titanium. On the other hand, the Ti He-α line is emitted in a high-temperature region (~1 keV).

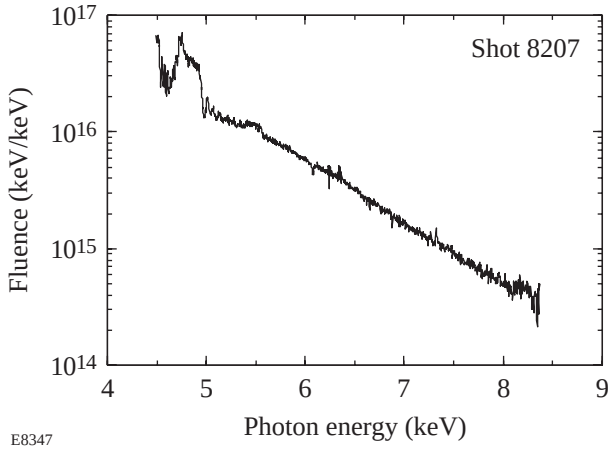

Figure 70.38
Calibrated, time-integrated x-ray spectrum obtained on shot 8207. Ti absorption lines are seen around 4.6 keV and the Ti *K* edge at 4.966 keV. These absorptions take place when the radiation emitted by the hot, compressed core is absorbed by the colder Ti layer within the shell.

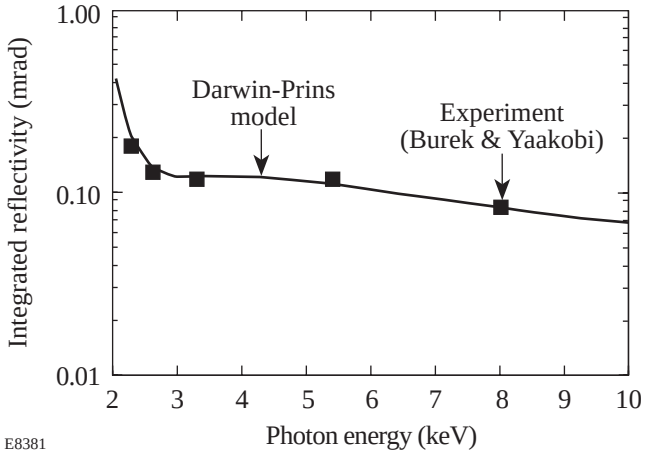

Figure 70.39
Measured[12] and calculated[13] integrated reflectivity of Ge(111) crystal.

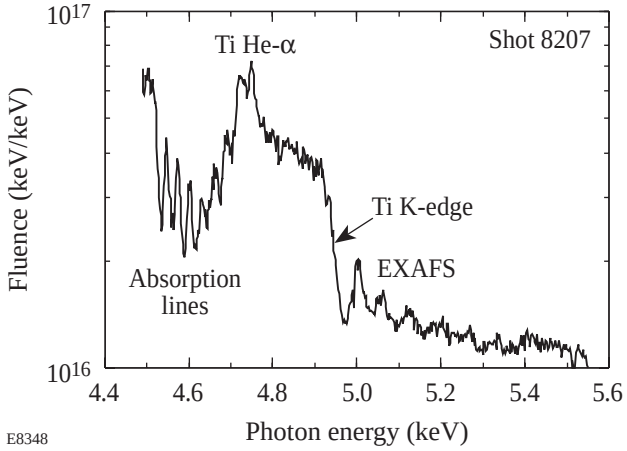

Figure 70.40
Part of the spectrum of Fig. 70.38, where absorption features appear. The lines around 4.6 keV are absorbed within a cool titanium layer (T_e ~200 to 500 eV), whereas radiation above the Ti *K* edge at 4.966 keV is absorbed by much colder titanium. The EXAFS oscillations also indicate cold titanium. On the other hand, the Ti He-α line is emitted in a high-temperature region.

K-Edge Absorption

The spectrum shows a drop in intensity at the *K* edge of cold titanium at 4.966 keV. This indicates the existence of cold titanium around the time of peak compression, when the observed core emission of continuum radiation is significant. To estimate the temperature of the absorbing titanium we note that for each electron ionized from a titanium atom, the *K* edge shifts to higher energies. A simple method for estimating the energy of these edges is discussed in Ref. 14. When the 12 *M*-shell electrons in Ti are removed, the edge shifts progressively from 4.966 keV up to about 5.2 keV; when the eight *L*-shell electrons are removed, the edge shifts progressively from ~5.2 to ~6.2 keV. The sharpness of the *K*-edge absorption indicates that no more than a few *M*-shell electrons are ionized, indicating a temperature lower than ~10 to 20 eV. The EXAFS spectrum discussed below indicates a still lower temperature.

The drop above the *K* edge corresponds to an absorption by a cold titanium layer of an areal density of 1.3 mg/cm^2

(equivalent to a 2.9-μm-thick solid titanium foil). This is 9.3 times higher than the original areal density of the titanium layer, 0.135 mg/cm^2. Using this value of areal density we can derive the spectrum emitted by the core before being attenuated by the cold titanium layer. This is simply given by $I(E)/\exp\left[-\rho\Delta r\ \tau(E)\right]$, where $I(E)$ is the observed spectrum and $\tau(E)$ is the absorption (or opacity) of cold titanium; the result is shown in Fig. 70.41. The continuum is indeed seen to fall along a smooth exponential curve whose slope indicates a core electron temperature of 0.94 keV. This could have also been deduced from the high-energy part of the continuum in Fig. 70.38, where the attenuation by the cold titanium is negligible.

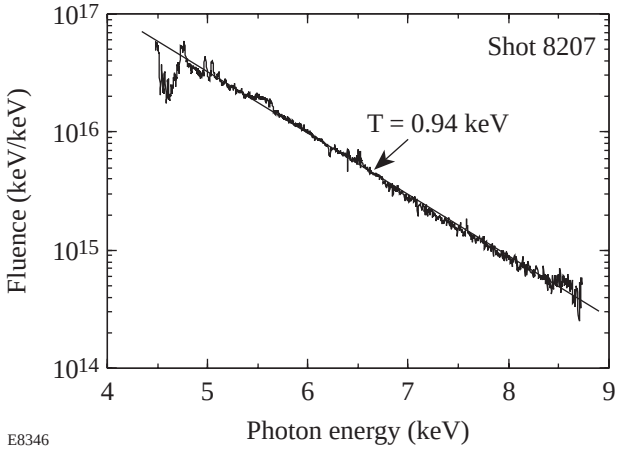

Figure 70.41
The calculated core emission before being absorbed by the cold titanium layer. The core electron temperature obtained by the continuum slope is 0.94 keV.

EXAFS Spectrum

Above the K edge the spectrum shows oscillations due to EXAFS. EXAFS[15] is observed in solids (even amorphous ones) and is due to the interference of the photoelectron waves emitted from the absorbing ion and those reflected from the neighboring ions. It was previously observed in laser-heated flat targets[16] but not in imploded targets. The analysis of the EXAFS oscillations yields the interparticle distance and, hence, the density. EXAFS data for solid titanium have been published[17–19] and can be used for comparison.

The theory of EXAFS[15] yields an expression for $\chi(k) = \mu(k)/\mu_0(k) - 1$, where $\mu(k)$ is the absorption (or opacity) and $\mu_0(k)$ is the absorption of the isolated atom (i.e., without the EXAFS oscillations). The wave number of the ejected photoelectron k is given by $h^2k^2/2m = E - E_K$, where E is the absorbed photon energy and E_K is the energy of the K edge. The expression for $\chi(k)$ is

$$\chi(k) = \sum_j N_j F_j(k) \exp\left[-2\sigma^2k^2 - 2R_j/\lambda(k)\right] \times \sin\left[2kR_j + \phi_j(k)\right]/kR_j^2, \quad (1)$$

where N_j is the number of atoms surrounding the absorbing atom at a distance R_j. The backscattering amplitude $F_j(k)$ and phase shift factor $\phi_j(k)$ for titanium were taken from the detailed calculations by Teo and Lee,[20] and the mean free path of the ejected electron in titanium, $\lambda(k)$, was taken from calculations of Blanche *et al.*[17] The vibration amplitude σ^2 in the Debye-Waller factor and the interparticle distance R_j will be adjustable parameters in fitting the experimental EXAFS spectrum to Eq. (1).

Figure 70.42 shows the calculated absorption $\mu(k)$ of the cold titanium layer in shot 8207 (shown above to have an areal density of 1.3 mg/cm^2), compared with an EXAFS spectrum of a 6-μm titanium foil absorber, obtained with synchrotron irradiation.[19] The latter curve was multiplied by the ratio of thicknesses (2.9/6) in order to normalize it to the effective thickness (2.9 μm) of the absorbing layer in shot 8207. For both curves, the absorption was reduced by the much smaller absorption due to L-shell electrons, given by the absorption below the K edge (thus the absorption curves equal zero below the edge). The oscillations in the present result have a slightly larger period (thus a smaller R) and larger amplitude than the solid-titanium oscillations; both are consistent[21] with slightly

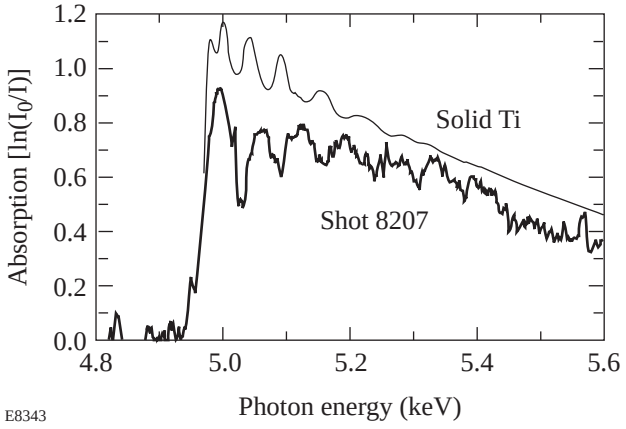

Figure 70.42
Comparison of the absorption due to the cold titanium layer in shot 8207 and in a 6-μm-thick solid titanium foil, irradiated by synchrotron radiation. The latter curve was normalized to the effective thickness (2.9 μm) of the titanium layer in shot 8207.

higher than solid density in our case. The more gradual rise above the *K* edge in the curve obtained here is partly the result of finite spectral resolution and partly due to the ionization of a few *M*-shell electrons.

The isolated-atom absorption curve $\mu_0(k)$ is given by a smooth average through the EXAFS oscillations; thus, the ratio $\chi(k) = \mu(k)/\mu_0(k) - 1$ retains the changes in the absorption due only to the EXAFS oscillations. Before fitting the experimental EXAFS spectrum to Eq. (1), a Fourier transformation is applied (yielding the radial charge distribution around the absorbing atom) to single out the contribution of only the first term in Eq. (1), that of the closest shell of atoms around the absorbing atom. Also, rather than transforming $\chi(k)$, the quantity $k^3\chi(k)$ is normally chosen,[15] putting more weight on the part of the spectrum away from the *K* edge (i.e., on higher *k* values). This choice is advantageous because Eq. (1) is imprecise at small *k* values; also, the effect of uncertainty in the value of E_K (due to valence-band energy structure) diminishes with increasing *k* values. The range of 2 to 10 Å^{-1} was used for the analysis of $k^3\chi(k)$. Below 2 Å^{-1} the curve is negligibly small; above $k \sim 10$ Å^{-1} the EXAFS spectrum is obscured by the rise of the Ti He-β line (albeit weak) at 5.582 keV and its dielectronic satellites.

The result of Fourier transforming the quantity $k^3\chi(k)$ (using a Hanning window[22] to avoid spurious oscillations) is seen in Fig. 70.43. Only one peak, at 2.2 Å, has a significant contribution. This distance is not exactly equal to the interparticle distance because of the effect of the phase factor $\phi_j(k)$ in Eq. (1). We next filter out this peak (extending from ~1 to ~3 Å) by multiplying the curve of Fig. 70.43 by an appropriate super-Gaussian curve, and finally apply an inverse Fourier transformation back to the *k* space. The resulting curve (Fig. 70.44) was fitted by the first term of Eq. (1), multiplied by k^3. As mentioned above, the functions $F(k)$, $\lambda(k)$, and $\phi_j(k)$ for titanium have been calculated in great detail, and thus the two remaining parameters, σ^2 and *R*, serve as adjustable parameters in the fit; no additional normalization was applied. Figure 70.44 shows the best fit, with $\sigma^2 = 0.013$ Å^2 and $R = 2.6$ Å. The parameter *R* depends primarily on the oscillation frequency of $k^3\chi(k)$, whereas σ^2 depends primarily on the amplitude decay rate at large *k* values (the amplitude rises at small *k* values because of the k^3 factor). Additionally, σ^2 determines the location and magnitude of the maximum in the $k^3\chi(k)$ curve. It should be emphasized that no amplitude normalization was applied to obtain this fit.

In solid titanium each atom is surrounded by two sub-shells of six atoms each, at distances of 2.889 Å and 2.940 Å. The unresolved peak in Fig. 70.43 thus corresponds to $N = 12$ backscattering atoms at an average distance of 2.6 Å [hence the choice $N = 12$ in Eq. (1)]. This indicates a titanium layer of density ~1.4 higher than that of solid titanium, i.e., a density of 6.4 g/cm^3. The Debye-Waller parameter σ (the amplitude of ion thermal oscillations) is proportional to $T_i^{1/2}$. By comparison with room-temperature EXAFS spectra of titanium, the spectrum of Fig. 70.44 corresponds to an ion temperature below ~1 eV. The values of density and temperature deduced here from the EXAFS spectrum are similar to those found with

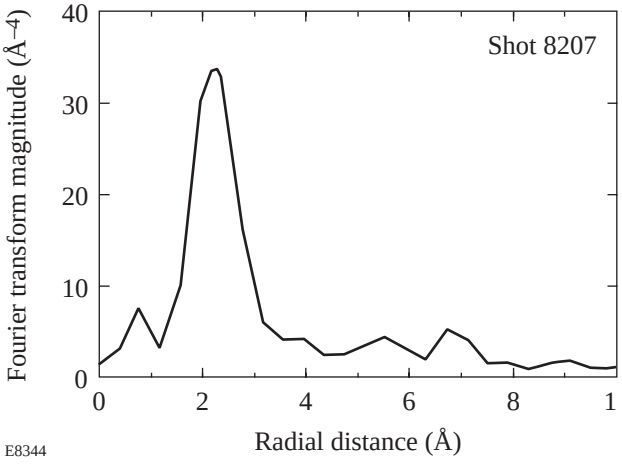

Figure 70.43
The result of Fourier transforming the $k^3\chi(k)$ curve obtained from Fig. 70.42. The peak at 2.2 Å corresponds to the shell of ions closest to the ion absorbing the photon.

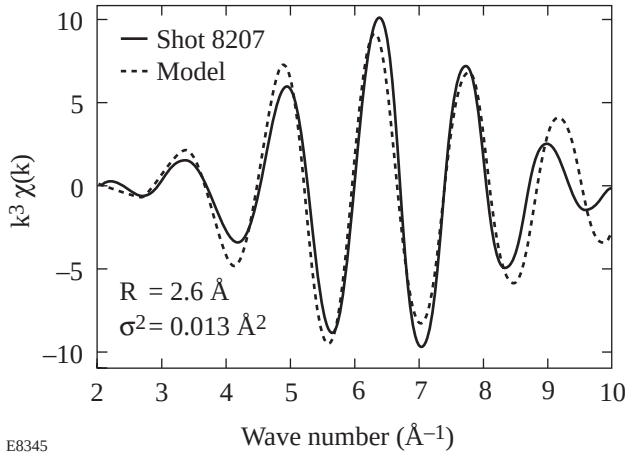

Figure 70.44
Fitting Eq. (1) to the experimental $k^3\chi(k)$ curve, obtained by the inverse Fourier transform of the curve in Fig. 70.43. Two adjustable parameters were used (interparticle distance *R* and Debye-Waller amplitude σ^2) with no additional normalization.

an EXAFS measurement of laser-compressed foils.[16] However, the ion temperature deduced here is lower than the electron temperature estimated above (T_e < 10 to 20 eV) from the sharpness of the *K*-edge absorption.

Absorption Lines

The absorption lines seen in Fig. 70.40 indicate that part of the titanium shell is ionized, in addition to the cold part giving rise to the *K*-edge and EXAFS absorptions. The application of absorption lines to determine the properties of the compressed shell was discussed in detail in Ref. 2. We show in Fig. 70.45 an expanded view of the absorption-line manifold obtained on shot 8207, compared with opacity calculations for $T = 300$ eV and $\rho = 6.4$ g/cm^3. The calculations were taken from the LTE opacity library OPLIB,[23] which was also used in the simulations described in the next section. The validity of assuming LTE populations in the calculation of absorption lines has been discussed in Ref. 2. The absorption lines around 4.6 keV correspond to transitions of the type 1*s*–2*p* in titanium ions of an incomplete *L* shell: Ti^{+13} to Ti^{+20}, formed when core-emitted continuum traverses the cold titanium layer. The designation Li in Fig. 70.45 stands for lithium-like titanium ion, and likewise for the other designations. Each peak contains several lines that are unresolved mostly because of broadening due to the finite source size. For example, the peak marked C (carbon-like) consists of 35 transitions of the type $1s^22s^22p^2$–$1s2s^22p^3$. The intensity distribution of the absorption peaks depends mostly on the temperature but also on the density. For example, the cases where the dominant peaks are the C-like or the N-like peaks (as in shot 8207) correspond to a temperature that changes from ~200 to ~500 eV for an assumed density in the range of 1 to 50 g/cm^3. Thus, with no knowledge of the density, a comparison as in Fig. 70.45 can be used to obtain only a rough estimate of the temperature in the cold shell. The energies calculated by OPLIB are approximate, and Fig. 70.45 shows them to be slightly different than the measured values.

In addition to absorption lines, Fig. 70.45 shows the emission of the He-α line of Ti^{+20}. The emission of He-like lines from a doped layer that is sufficiently removed from the interface was shown[1] to be a signature of mixing. Indeed, code simulations described in the next section show that these lines *should not have been seen* in the spectrum, in the absence of mixing.

Next we deduce the shell areal density from the absorption lines, using the relation[2]

$$\int \ln\left[I_0(E)/I(E)\right]dE = \rho\Delta r \int k(E)dE \; . \qquad (2)$$

The left-hand term is an integral over the measured absorption-line manifold [if film density is proportional to ln(*I*), this term equals the area enclosed within the absorption lines in a film-density plot]. Although the opacity integral depends on the temperature and density of the absorbing region, it has been shown[2] that using the observed intensity distribution of the absorption peaks enables us to deduce the areal density without having to know these parameters. We calculate the opacity integral $\int k(E)dE$ for titanium, using the OPLIB opacity library,[23] for a wide range of temperatures and densities. When the results are grouped by the peak of highest opacity, the integral values fall within relatively narrow ranges, which can be understood as follows: Ionization increases with increasing

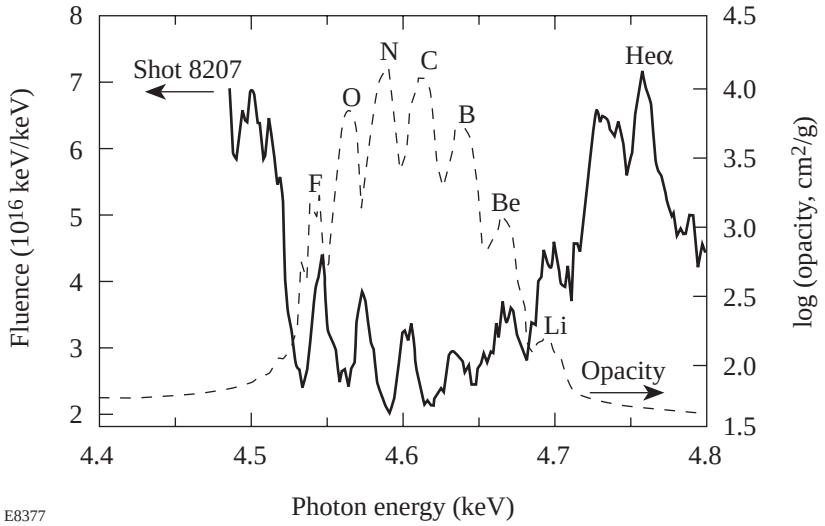

Figure 70.45
Comparison between the measured Ti absorption lines from shot 8207 and the opacity calculated by OPLIB. The OPLIB calculation is for $T = 300$ eV and $\rho = 6.4$ g/cm^3. The designation Li stands for 1*s*–2*p* transitions in Li-like Ti, and likewise for the other designations.

temperature but decreases with increasing density (because the three-body recombination rises faster with density than other, two-body processes). Thus, a given ionization level is obtained for pairs of (T,ρ) values where both increase simultaneously. Since opacity increases with density but decreases with temperature, the integrated opacity for such pairs tends to be reasonably constant. We show in Fig. 70.46 the calculated opacity integral, arranged according to the strongest opacity peak (marked Li for cases where the lithium-like peak is the strongest, etc.). Thus, simply knowing the strongest absorption peak narrows down the uncertainty in the integrated opacity and, hence, in the deduced areal density. For example, for cases where the C-like peak is the strongest, the uncertainty in the integrated opacity is ±25%. Applying Fig. 70.46 and Eq. (2) to the spectrum of shot 8207, we find $\rho\Delta r \sim 0.4$ mg/cm^2 for the titanium layer with a temperature in the range of ~200 to 500 eV. Adding the areal density found above for the cold titanium (1.3 mg/cm^2), we find a total $\rho\Delta r$ for the titanium layer of 1.7 mg/cm^2. In adding the areal densities we have assumed that the line- and *K*-edge absorptions occur at the same time, signifying a temperature gradient within the titanium layer. This is indeed indicated by Fig. 70.40. Suppose the two absorptions take place at two different times: the *K* edge is absorbed at time t_1 and the lines are absorbed at a time t_2. The observed fluence above the *K* edge (~1.2×10^{16} keV/keV) consists then of three parts: (a) the fluence that was emitted at t_1 but survived the *K*-edge absorption, (b) the fluence emitted at t_2, and (c) the fluence emitted at other times. Thus, the fluence at t_2 must be smaller than the observed fluence above the *K* edge. However, this level of fluence is much smaller than the depth of the absorption lines (~4×10^{16} keV/keV), indicating insufficient fluence to absorb the lines in those times.

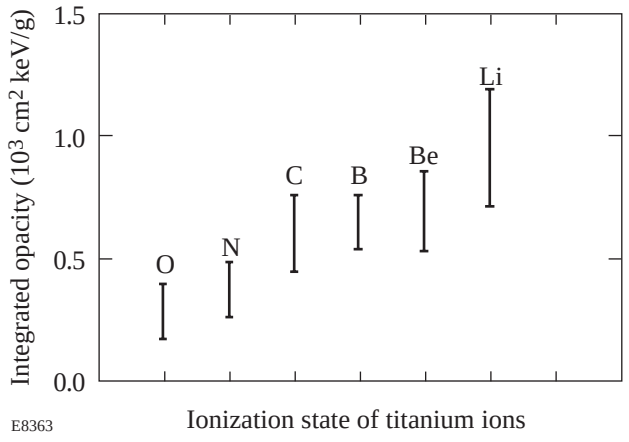

Figure 70.46
Area under the opacity-spectrum peaks of titanium (corresponding to the absorption-line manifold around 4.6 keV). For temperatures in the range of 300 to 1000 eV and densities in the range of 1 to 50 g/cm^3, the points are grouped according to the strongest absorption peak in the opacity spectrum (Li stands for cases where the lithium-like peak is the strongest, and likewise for the other designations).

Using the measured $\rho\Delta r$ of the titanium layer we can estimate the $\rho\Delta r$ of the entire compressed shell. Figure 70.47 shows the ratio $Q = (\rho\Delta r)_{\text{total}} / (\rho\Delta r)_{\text{Ti}}$ calculated by the one-dimensional hydrodynamic code *LILAC*[24] for shot 8207 as a function of the compression ratio (defined as r_0/r, where r is the radius of the gas-shell interface and r_0 is its initial value). Also shown is the result of a simple geometrical model where the unablated part of the shell is assumed to be incompressible as it implodes inward. Since charge-collector measurements (and simulations) indicate that an overcoat thickness of ~9 μm is ablated, the model uses the inner 10.9 μm as the unablated part of the shell. Thus, a lower bound $Q \sim 10$ can be used, giving $\rho\Delta r > 17$ mg/cm^2 for the compressed shell.

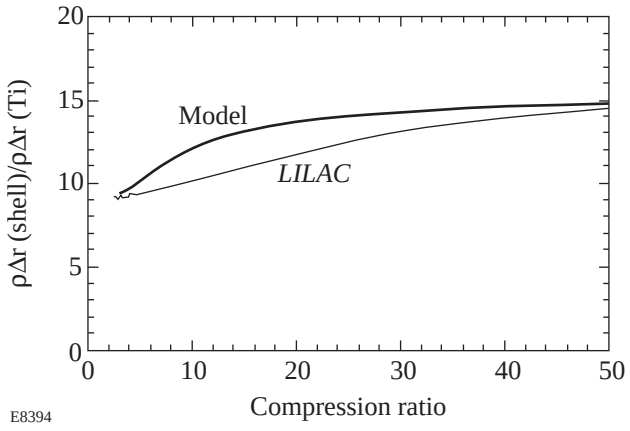

Figure 70.47
The ratio of $\rho\Delta r$ for the total shell and for the titanium layer. The model assumes that the unablated shell implodes incompressibly. The compression ratio is defined as r_0/r, where r is the radius of the gas-shell interface and r_0 is its initial value.

It should be pointed out that the use of time-integrated spectra yields an underestimate of the areal density because emission during times when absorption is insignificant diminishes the absorption contrast (typically[2] by a factor of ~2).

Comparison with Simulations

In this section we compare the observed spectrum with that predicted by *LILAC*.[24] The Ti spectral signatures are shown to reflect the reduced target performance that was a consequence of the poor irradiation uniformity in this experiment.

The simulated spectra were computed by applying a radiation-transport model[1] to *LILAC*-generated profiles, using the OPLIB opacity library. As discussed elsewhere,[1,2] using the LTE opacity library is adequate for simulating the continuum radiation and the absorption lines. However, this would not be true for simulating the emission of helium-like and hydrogen-like titanium lines.

Figure 70.48 shows the comparison for the higher-energy part of the spectrum, and Fig. 70.49 the lower-energy part, where the absorption features appear. In both cases the simulated spectra are integrated in time up to the time marked in Figs. 70.48 and 70.49. The integration up to 2 ns is essentially an integration over the whole implosion. The simulated curves show some flattening below ~7 keV due to shell attenuation,[25,9] and only higher-energy radiation is unattenuated and can be used to determine the core temperature. However, the experimental curve does not show this flattening, indicating a less-compressed shell. It also shows a cooler core than predicted: T = 0.94 as compared with T = 1.8 keV. The maximum temperature in the simulation (T ~ 3 keV) was higher than that indicated by the time-integrated continuum slope (T = 1.8 keV), and thus it can be expected that the peak temperature in this experiment is ≳1 keV. The lower tempera-

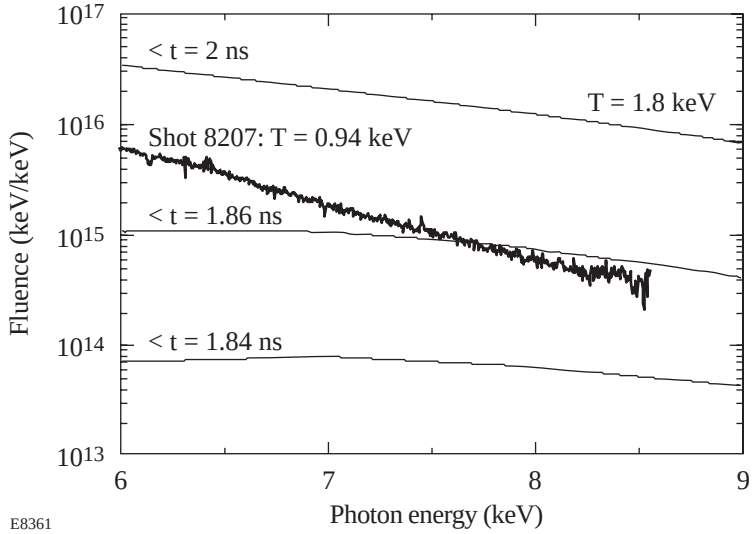

Figure 70.48
Comparison of the measured and simulated x-ray continuum spectra for shot 8207. The simulated curves are integrated up to the marked times. The slopes yield the core electron temperature.

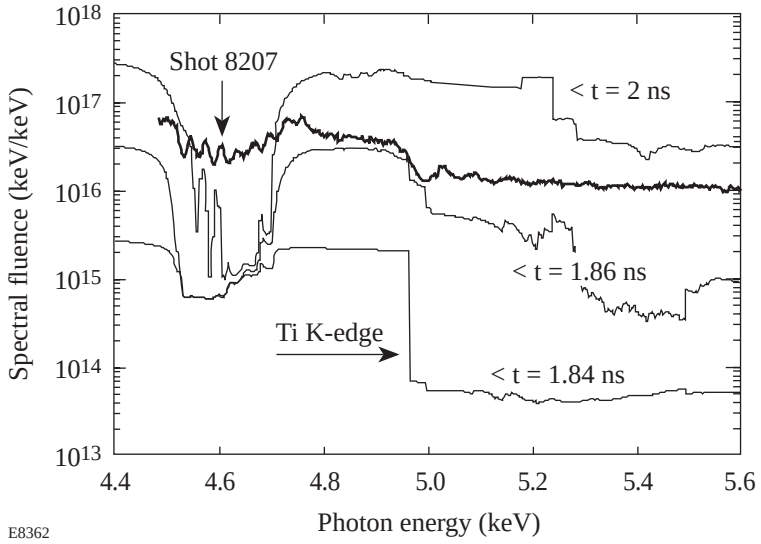

Figure 70.49
Comparison of measured and simulated x-ray spectra for shot 8207, in the region showing absorption features. The simulated curves are integrated up to the marked times.

ture and compression result in a much lower core-radiation fluence than predicted. Figure 70.48 shows that the implosion in this experiment falls short of the 1-D code predictions; in particular, the target fails to undergo the final compression stage that is predicted to occur between ~1.86 ns and peak compression at ~1.9 ns.

Similar conclusions can be drawn from the comparison in Fig. 70.49. The simulated time-integrated spectrum (<2 ns) shows much deeper absorption lines than observed, indicating a higher areal density, and little *K*-edge absorption, indicating a higher shell temperature. In fact, the saturated absorption of the simulated absorption lines shows that almost all radiation emitted after ~1.84 ns at the wavelengths of these lines is absorbed. As time progresses, the simulated spectra show a gradual shift from *K*-edge absorption to line absorption, indicating heating of the titanium layer by the core. Also, the absorption-line manifold is seen to shift toward higher ionizations, again indicating an increase in shell temperature. By contrast, the experimental curve shows (a) a lower total absorption, indicating a lower areal density [see Eq. (2)], and (b) prominence of *K*-edge absorption over line absorption, indicating a cooler shell. As in Fig. 70.48, the results show that the implosion is effectively aborted after ~1.86 ns. At intermediate times (~1.84 to 1.86 ns) *K*-edge and line absorptions occur simultaneously, which was shown above to be the case in the experiment.

We also note absorption features above ~5 keV in the simulated spectra but not in the measured spectrum. These are *K*-edge absorption in ionized Ti, as well as transitions of the type 1*s*–3*l* (*K*-shell to *M*-shell transitions) in various titanium ions.

The measured $\rho\Delta r$ of the titanium layer was found above to be ~1.7 mg/cm^2. The same $\rho\Delta r$ value in the simulation occurs at 1.7 ns, consistent with the conclusion of incomplete compression suggested above. At 1.7 ns the predicted titanium density is 11 g/cm^3, compared with the value 6.4 g/cm^3 deduced from the EXAFS spectrum. The predicted electron temperature is ~50 eV, compared with the estimate T <10 to 20 eV from the sharpness of the *K*-edge absorption. The simulated spectra also predict no emission of helium-like Ti lines (even though LTE opacity modeling tends to overestimate their intensity).

The appearance of the He-α line in the experiment (see Fig. 70.45) is clear evidence of shell-core mixing,[1] which transports titanium into high-temperature regions. Titanium can be driven out to the ablation region (during acceleration) or into the compressed core (during deceleration). To determine which is the case in this experiment, we examine the spatial profile of the He-α line, as measured by the crystal spectrometer. Figure 70.50 shows the profiles (in the target plane) at the wavelength of the He-α line, as well as at a nearby wavelength; the net He-α emission is given by their difference. The sharpness of the core emission profile indicates a smaller core than the slit width (100 μm), consistent with the 60-μm width measured by the x-ray microscope. Figure 70.50 clearly shows that most of the He-α emission comes from the core, indicating mixing during the deceleration phase. The peak core temperature ($\gtrsim$1 keV) is sufficiently high to excite the He-α line. The observed intensity of the He-α line can be used to obtain a rough estimate of the amount of titanium reaching the core due to mixing. To that end, we repeat the simulations of Fig. 70.49 while assuming that a small fraction of the titanium mass is uniformly spread throughout the shell layers lying inward of the original titanium layer. Figure 70.51 shows the result for the case of mixing 3% of the total titanium mass into the core. The He-α line (as well as its adjacent satellite line) now appears in the calculated spectrum. A comparison is made between the experimental spectrum and the simulated spectrum integrated up to 1.86 ns, as suggested by Figs. 70.48 and 70.49. In calculating the spectrum of Fig. 70.51, a correction was made to account for the LTE calculations' overestimate of the intensity of the emission lines. A steady-state, non-LTE model was used to calculate the relative populations of the lithium-like, helium-like, and hydrogen-like Ti species, from which the intensity of the major

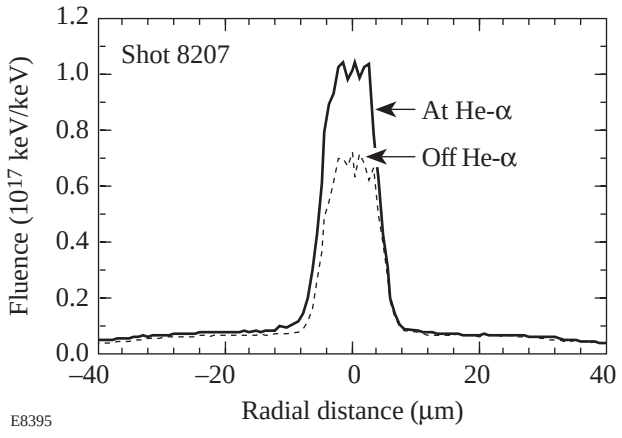

Figure 70.50
Spatial profile of emission at the wavelength of the Ti He-α line (4.75 keV), and at a nearby wavelength. The difference (i.e., the net He-α emission) indicates mixing of titanium into the compressed core.

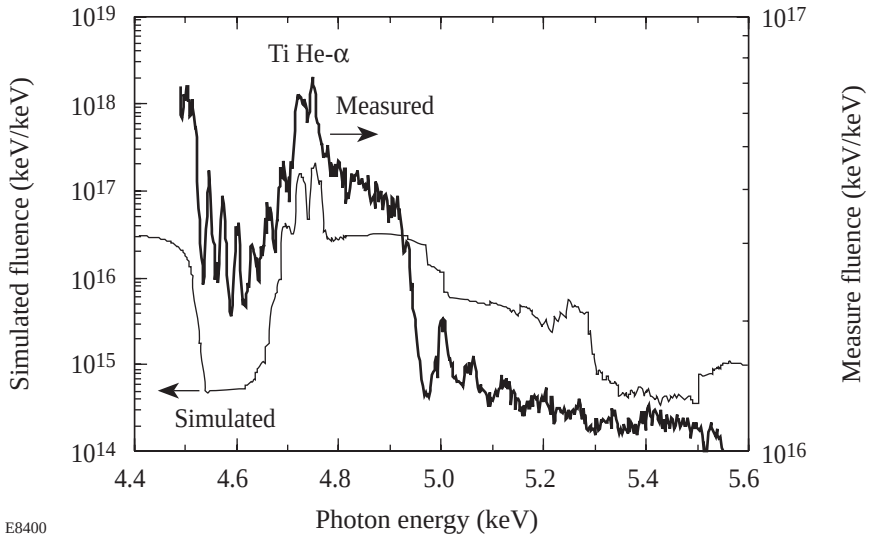

Figure 70.51
Simulation of mixing: the simulated curve (integrated up to 1.86 ns) assumes that 3% of the total titanium mass is uniformly spread throughout the shell layers inward from the original titanium layer. Note the appearance of the He-α line due to mixing, in agreement with the time-integrated, measured spectrum.

lines due to collisional excitation follows. The required ionization, recombination, and excitation rates were taken from Ref. 26.

The reduced target performance evidenced in Figs. 70.48 and 70.49 as well as the presence of mixing is the result of inadequate irradiation uniformity when not using phase plates to smooth the laser irradiation, as well as the result of the density jump at the titanium layer interfaces. The titanium spectral signatures studied in this work should prove very useful in tracking the improved target performance with improved laser uniformity.

ACKNOWLEDGMENT

This work was supported by the U.S. Department of Energy Office of Inertial Confinement Fusion under Cooperative Agreement No. DE-FC03-92SF19460, the University of Rochester, and the New York State Energy Research and Development Authority. The support of DOE does not constitute an endorsement by DOE of the views expressed in this article.

REFERENCES

1. B. Yaakobi, R. S. Craxton, R. Epstein, and Q. Su, J. Quant. Spectrosc. Radiat. Transfer **55**, 731 (1996).

2. Laboratory for Laser Energetics LLE Review **69**, NTIS document No. DOE/SF/19460-152, 1996 (unpublished), p. 11.

3. A. Hauer, R. D. Cowan, B. Yaakobi, O. Barnouin, and R. Epstein, Phys. Rev. A **34**, 411 (1986).

4. L. D. Landau and E. M. Lifshitz, *Fluid Mechanics*, 2nd ed. (Pergamon Press, New York, 1987), p. 36.

5. T. R. Boehly, R. S. Craxton, T. H. Hinterman, J. H. Kelly, T. J. Kessler, S. A. Kumpan, S. A. Letzring, R. L. McCrory, S. F. B. Morse, W. Seka, S. Skupsky, J. M. Soures, and C. P. Verdon, Rev. Sci. Instrum. **66**, 508 (1995).

6. D. K. Bradley, T. Boehly, D. L. Brown, J. Delettrez, W. Seka, and D. Smith, in *Laser Interaction and Related Plasma Phenomena*, edited by H. Hora and G. H. Miley (Plenum Press, New York, 1991), Vol. 9, pp. 323–334.

7. Laboratory for Laser Energetics LLE Review **37**, NTIS document No. DOE/DP40200-83, 1988 (unpublished), p. 29; *ibid*., p. 40.

8. Laboratory for Laser Energetics LLE Review **33**, NTIS document No. DOE/DP40200-65, 1987 (unpublished), p. 1.

9. F. J. Marshall, J. A. Delettrez, R. Epstein, and B. Yaakobi, Phys. Rev. E **49**, 4381 (1994).

10. Laboratory for Laser Energetics LLE Review **64**, NTIS document No. DOE/SF/19460-99, 1995 (unpublished), p. 145.

11. B. L. Henke *et al*., J. Opt. Soc. Am. B **3**, 1540 (1986).

12. A. J. Burek and B. Yaakobi, Final Report to the National Bureau of Standards contract NB81NAHA2032, 1983 (unpublished), Appendix A.

13. B. L. Henke, E. M. Gullikson, and J. C. Davis, At. Data Nucl. Data Tables **54**, 181 (1993) (Note: the Ge data is referenced on p. 327).

14. Laboratory for Laser Energetics LLE Review **49**, NTIS document No. DOE/DP40200-188, 1991 (unpublished), p. 1.

15. P. A. Lee *et al*., Rev. Mod. Phys. **53**, 769 (1981).

16. R. W. Eason, D. K. Bradley, J. D. Kilkenny, and G. N. Greaves, J. Phys. C, Solid State Phys. **17**, 5067 (1984); A. Djaoui *et al*., Plasma Phys. Control. Fusion **31**, 111 (1989); B. A. Shiwai *et al*., Laser Part. Beams **10**, 41 (1992).

17. G. Blanche *et al.*, Ultramicroscopy **50**, 141 (1993).

18. D. Denley *et al.*, Phys. Rev. B **19**, 1762 (1979); G. Blanche *et al.*, J. Phys. IV **4**, 145 (1994).

19. A. Balzarotti, M. De Crescenzi, and L. Incoccia, Phys. Rev. B **25**, 6349 (1982).

20. B.-K. Teo and P. A. Lee, J. Am. Chem. Soc. **101**, 2815 (1979).

21. R. C. Albers, A. K. McMahan, and J. E. Müller, Phys. Rev. B **31**, 3435 (1985).

22. A. V. Oppenheim and R. W. Schafer, *Digital Signal Processing* (Prentice-Hall, Englewood Cliffs, NJ, 1975), Chap. 5.

23. M. F. Argo and W. F. Heubner, J. Quant. Spectrosc. Radiat. Transfer **16**, 1091 (1976).

24. Laboratory for Laser Energetics Report No. 16, 1983 (unpublished); Laboratory for Laser Energetics LLE Review **36**, NTIS document No. DOE/DP40200-79, 1986 (unpublished).

25. B. Yaakobi, R. Epstein, and F. J. Marshall, Phys. Rev. A **44**, 8429 (1991).

26. R. C. Elton, in *Plasma Physics*, edited by H. R. Griem and R. H. Loveberg, Methods of Experimental Physics, Vol. 9A (Academic Press, New York, 1970), pp. 115–168.